Structure and Rheological Properties of Latex−Silica Nanocomposite Films: Stress−Strain Isotherms

Julian Oberdisse

Laboratoire Léon Brillouin, CEA/CNRS, CEA Saclay, 91191 Gif sur Yvette Cedex, France

Received April 24, 2002

ABSTRACT: A study of the rheological properties of silica-filled nanolatex films by means of uniaxial strain experiments is presented. The samples are made by evaporating the aqueous solvent of mixtures of colloidal silica and colloidal nanolatex, followed by film formation. The reinforcement effect due to the introduction of hard silica beads is investigated as a function of silica volume fraction Φ, pH in solution before film formation, and silica bead size. The stress−strain curves show that the material can be stretched up to high elongations λ typically around four or more before rupture, indicating that the extensibility of the pure nanolatex film is conserved. It is found that the silica contributes differently at small and large deformations: In the small deformation regime ($\lambda \leq 1.2$), considerable reinforcement (a factor of 10 in Young's modulus with respect to the pure nanolatex) is obtained with silica volume fractions of the order of 10%. At higher elongations, the reinforcement factor decreases, and the rheology of the nanocomposite samples approaches that of the pure nanolatex films.

I. Introduction

Reinforcement of elastomers with hard fillers is a common procedure for optimization of rheological properties.[1−6] Many ways of incorporating the filler in the polymer bulk exist, the most popular being mechanical mixing (milling). Other, usually more complex routes are in situ filler synthesis[7−10] or polymerization around the filler particles.[11] The rheological properties of the resulting composites are in general complex, e.g., they may show strain-softening, hysteresis, or aging effects, and are difficult to describe theoretically.[12−15] It is therefore often impossible to determine the mechanisms of reinforcement. Among other reasons, this might be due to the lack of structural information on the scale of the reinforcing objects, although some pioneering studies exist.[7,8,16,17]

We have recently employed a different method of preparation of nanocomposite samples. It consists of mixing colloidal solutions of nanolatex and silica in the desired proportions, adjusting the pH, and evaporating the aqueous solvent; cf. for example refs 18 and 19. After film formation of the nanolatex[20−22] with the silica inclusions, we have analyzed the structure of the silica in the polymeric matrix by small-angle neutron scattering (SANS)[23] for different physicochemical conditions. In the present article, we discuss the results of uniaxial strain experiments with the same model nanocomposite samples. Note that the matrix is an entangled melt and not a rubber (no cross-links) and that our experiments are therefore of *rheological* nature. At the temperature of interest, however, the flow of the material is sufficiently slow and the observed reinforcement effects are sufficiently strong that our conclusions are nonetheless relevant for the *mechanical properties* of filled rubber as well.

The paper is organized as follows: In section II, we present experimental details about the samples and the rheological measurements. In section III, the stress−strain isotherms are presented for several series of samples, varying stock solution pH, silica volume fraction, and silica bead size. Results are discussed in section IV, where we confront the previously determined filler structure with the stress−strain isotherms.

II. Experimental Section

II.1. Sample Preparation. We briefly recall the sample preparation, which is presented in detail in ref 23. The basic idea is to mix two colloidal solutions and evaporate the solvent. The starting components are aqueous colloidal suspensions of silica from Akzo Nobel (two sizes, Bindzil 30/220 and Bindzil 40/130; hereafter called B30 and B40, respectively) and nanolatex polymer beads. The latter was kindly provided by Rhodia. It is a core−shell latex of copolymerized poly(methyl methacrylate) (PMMA) and poly(butyl acrylate) (PBuA), with a hydrophilic shell containing methacrylic acid. From the analysis of the form factors of silica and nanolatex measured separately by SANS in dilute aqueous solutions, we have deduced the following radii R_0 and polydispersities σ of a log-normal size distribution:[23] $R_0 = 76.9$ Å, $\sigma = 0.186$ (B30); $R_0 = 92.6$ Å, $\sigma = 0.279$ (B40); $R_0 = 138.9$ Å, $\sigma = 0.243$ (nanolatex). Colloidal stock solutions of silica and nanolatex are brought to desired concentration and pH, mixed, and degassed under primary vacuum in order to avoid bubble formation. Slow evaporation of the solvent at $T = 65$ °C under atmospheric pressure takes about 4 days, conditions which have been found suitable for the synthesis of smooth and bubble-free films without any further thermal treatment.

II.2. Stress−Strain Isotherms. Rectangular samples for rheological tests are cut at $T \approx 70$ °C into pieces of approximate dimensions 30 × 10 × 1 mm^3 and brought to constant thickness using sandpaper. They are glued with commercial cyanoacrylate on both ends on emery paper, on which the clamps of the homemade mechanical stretching apparatus are fixed. Samples are subjected to a very slight tension, leading to an offset of at most 0.05 MPa in initial tension, and immerged in silicon oil at $T = 60.0$ °C, well above the glass transition temperature of the matrix of $T_g = 33$ °C, measured by Rhodia (DSC). After a short thermal equilibration time of about 30 s, the samples are stretched up to rupture. The deformation in a constant rate setup ($\dot{\gamma} = 0.0016$ s^{-1}) is controlled. The relative elongation $\lambda = L(t)/L_0$, where L_0 is the initial sample length, is thus exponential: $\lambda = \exp(\dot{\gamma}t)$. This allows for a material test which is independent of the exact

10.1021/ma020635d CCC: $22.00
Published on Web 11/08/2002

value of the initial length. The force $F(\lambda)$ is measured with a HBM Q11 force transducer and converted to (real) stress inside the material σ:

$$\sigma(\lambda) = \frac{F(\lambda)\lambda}{A_0} \tag{1}$$

Here A_0 is the cross section of the undeformed film and the multiplication with λ accounts for the decrease in cross section ($\propto 1/\lambda$) with increasing elongation. The film is supposed to deform homogeneously (which is true at least up to moderate elongations) and to be incompressible. The $\sigma(\lambda)$ curves are analyzed in terms of Young's modulus E, the elongation at rupture λ_{rupt}, and the total energy e per unit volume of sample supplied by the motor of the stretching machine up to rupture. The latter is given by summing the product of force and displacement during stretching:

$$e = \int_1^{\lambda_{rupt}} \frac{\sigma(\lambda)}{\lambda}\, d\lambda \tag{2}$$

Tests of selected samples identical in composition have shown that our stress−strain results are trustworthy. Up to moderate strain, the stress of four samples cut from the same piece of film superimposes within about 10%; the statistical error bar in σ is thus well below the effects discussed in this paper. At large strain, the exact moment of rupture λ_{rupt} is reproducible within 15%. Note that rupture usually takes place at the clamps, indicating heterogeneous deformation in the final stages. In some cases differences are observed between films having the same nominal composition, but which are made from different stock solutions and/or made at different times. We will comment on this problem in the Discussion.

II.3. Small-Angle Neutron Scattering. The structural characterization of the samples has been presented in our previous article.[23] Some additional spectra have been measured on instrument PACE at LLB, and results are reported in the present paper. Two configurations were used: a first one with wavelength 9.3 Å, sample-to-detector distance of 4.58 m, and a collimation distance of 5.00 m, and a second one with wavelength 5.1 Å, sample-to-detector distance of 1.13 m, and a collimation distance of 2.50 m. H_2O has been used as calibration standard.

III. Results

We will show that the rheological properties of the samples depend in a systematic manner on the physicochemical parameters: the pH of the solution before solvent evaporation and the type and quantity of silica beads. We will first discuss the rheology of pure latex films, and then the one of the nanocomposite films, along some selected lines in the phase diagram.

III.1. Pure Latex Films. The pH of the colloidal solution before film formation is a key parameter of the nanocomposite material. We know from the SANS data that it has a direct impact on the structure of the silica aggregates. To check whether the pH influences also the nanolatex matrix itself, we have measured the stress σ as a function of deformation λ for *pure* nanolatex films made from colloidal solutions of pH 3.1, 7.0, and 9.3. The results are shown in Figure 1. They demonstrate that the pH strongly influences the rheological properties: "acid" films (pH 3.1) have a Young's modulus of $E_{latex} = 0.45$ MPa, and the stress stays low (<2 MPa) up to very high extensions ($\lambda_{rupt} > 7$, not reached in the experiment). "Neutral" films (pH 7.0) have $E_{latex} = 1.05$ MPa and $\lambda_{rupt} \approx 5.2$, whereas "basic" films (pH 9.3) are tougher ($E_{latex} = 1.45$ MPa) and break earlier ($\lambda_{rupt} \approx 3.7$), at a rather high stress ($\sigma_{rupt} = 9$ MPa). The input in energy per unit volume needed to break the film (cf. eq 2) is therefore more than a factor of 3 higher at pH 9.3 ($e \approx 3.1$ J/cm^3) than what can be estimated for the sample at pH 3.1.

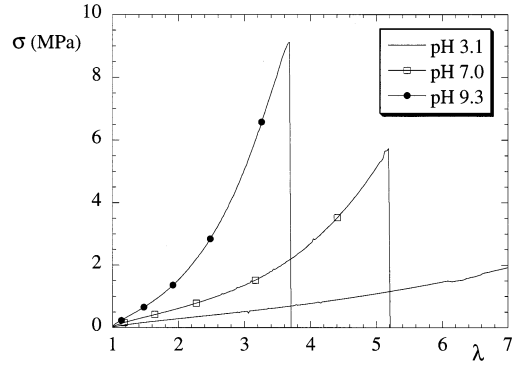

Figure 1. Stress σ in MPa as a function of relative elongation λ for pure nanolatex films from colloidal solution of pH 3.1, 7.0, and 9.3.

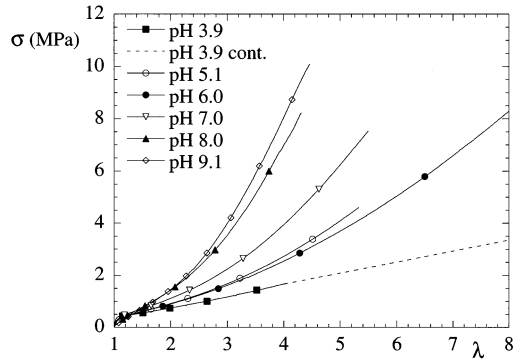

Figure 2. Stress σ in MPa as a function of relative elongation λ for nanocomposite films of silica B30 at $\Phi = 5.0\%$ for different pH values. Because of a problem in data acquisition, the $\sigma(\lambda)$ for pH 3.9 is incomplete. The film itself does not break before $\lambda = 8$. The dotted line is a plausible continuation.

III.2. Effect of pH on Nanocomposite Films. We start with the description of a series in pH at fixed volume fraction $\Phi = 5.0\%$ for films made with small silica beads (B30). The stress−strain curves $\sigma(\lambda)$ are shown in Figure 2. The stress of "acid" films increases little with deformation (up to $\sigma_{rupt} \approx 3$ MPa at pH 3.9), and they break at $\lambda_{rupt} > 8$. At intermediate pH values (pH 7), stress grows more and more, up to 7.5 MPa, and the rupture occurs earlier, around $\lambda_{rupt} \approx 5.5$. The samples at pH 5.1 and pH 6.0 have comparable stresses, the one at pH 5.1 being slightly higher. We will comment on this inversion in section IV.5. Basic films, pH 8.0 and 9.1, show a similar stress−strain curve, with a high stress between 8 and 10 MPa at rupture, around $\lambda_{rupt} \approx 4.3$. As a result, the energy input needed to break the films lies around $e \approx 4$ J/cm^3, whatever the pH of preparation.

In Figure 3, we focus on the small deformation region of the stress−strain isotherms shown in Figure 2. A clearly visible feature here is the considerable increase of Young's modulus with decreasing pH: from $E = 2.1$ MPa at pH 9.1 to $E = 4.8$ MPa at pH 7.0 and to $E = 10.6$ MPa at pH 3.9. Thus, Young's modulus changes by a factor of 5 from acid to basic pH for samples that contain the same quantity of silica. Moreover, the high value of Young's modulus of "acid" films together with their low overall stress leads to a remarkable change in slope at very low strain (at $\lambda = 1.05$). This feature disappears with increasing pH.

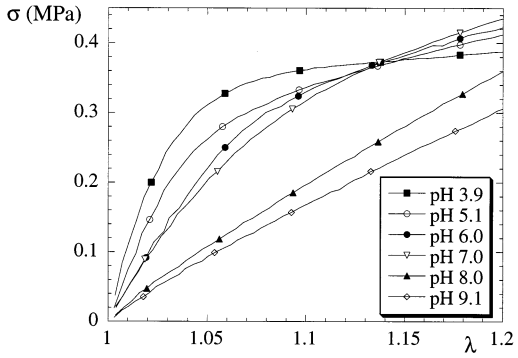

Figure 3. Stress σ in MPa as a function of relative elongation λ for the same samples as shown in Figure 2, in the low-deformation limit.

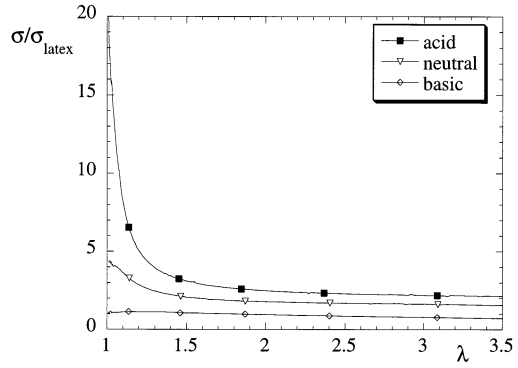

Figure 4. Reduced stress σ/σ_{latex} as a function of relative elongation λ for nanocomposite films of silica B30 at $\Phi = 5.0\%$ for pH 3.9, 7.0, and 9.1. See text for details.

One of the problems with the data plotted in Figures 2 and 3 is that we cannot unambiguously decide to what extent the observed sensitivity to pH is due to the nanolatex matrix or to the silica. An alternative presentation of the stress−strain isotherms is to compare them to the ones of the pure nanolatex films at the same pH. Our analysis is motivated by the equation given by Smallwood[24] for the modulus of a filled elastomer as a function of filler volume fraction. It is analogous to the equation originally proposed by Einstein[25] for the viscosity of a dilute colloidal solution. Formulated for Young's modulus E of the composite, it reads

$$E = E_{latex}(1 + 2.5\Phi + ...) \tag{3a}$$

E_{latex} is Young's modulus of the pure matrix. Extensions to higher volume fractions by including (pairwise) interactions between particles can be written

$$E = E_{latex}(1 + 2.5\Phi + B\Phi^2 + ...) \tag{3b}$$

where the prefactor of the second-order term has been evaluated—originally for the viscosity of a suspension—to $B = 14.1$.[26,27] To account for the often steep increase of the modulus with Φ, equations with an exponential increase have been proposed.[28] The simplest one with the same low Φ behavior as eq 3a reads

$$E = E_{latex} \exp(2.5\Phi) \tag{4a}$$

Other semiempirical equations have been proposed to account for percolation effects, usually by introducing a divergence in the modulus as Φ approaches the packing volume fraction Φ_{max}. The correction to eq 4a proposed by Mooney reads[28,29]

$$E = E_{latex} \exp\left(\frac{2.5\Phi}{1 - \frac{\Phi}{\Phi_{max}}}\right) \tag{4b}$$

The important point is that the Φ-dependent part of eqs 3 and 4, equal to E/E_{latex}, is the *factor of reinforcement* of the matrix by the filler. The analogous quantity here is the strain (and composition-)-dependent reduced stress $\sigma(\lambda)/\sigma_{latex}(\lambda)$. This normalization to the stress in the pure matrix is related to a commonly used representation of stress−strain data, the Mooney representation. It consists of normalizing the experimental stress by the theoretical stress−strain dependence of a phantom chain network (the "matrix"), proportional to $\lambda^2 - 1/\lambda$. The result, usually plotted vs $1/\lambda$, corresponds to the modulus. In our case, we take the experimental stress $\sigma_{latex}(\lambda)$ instead of the theoretical prediction. Using the reduced stress $\sigma(\lambda)/\sigma_{latex}(\lambda)$ has the advantage of canceling the pH dependence of the matrix, and the result can be interpreted as the reinforcement factor due to the filler structure only.

In Figure 4, we plot σ/σ_{latex} as a function of elongation for three samples ($\Phi = 5.0\%$) with different pH: pH 3.9, pH 7.0, and pH 9.1, as close as possible to the available pure nanolatex samples presented above (pH 3.1, pH 7.0, and pH 9.3). At basic pH, the stress in the composite and in the pure latex is almost identical up to $\lambda = 2$. Above this strain, the pure nanolatex film develops higher stress and breaks earlier. In Figure 4, this yields an essentially flat curve which starts from approximately one and then continuously decreases down to 0.7 at high λ. At pH 7.0, Young's modulus E of the nanocomposite film is a factor of 4.6 higher than the one of the pure film, and the stress in the nanocomposite stays higher over the whole range of λ. Note that the pure nanolatex film breaks again earlier. At acid pH finally (pH 3.1 and 3.9), E of the nanocomposite is more than 20 times higher than that of the pure nanolatex film, and the same behavior as at pH 7.0 is observed: The reduced stress falls off rapidly, down to a plateau value of 2.2, and the pure film breaks earlier.

We now turn to the analogous series at a *higher volume fraction* $\Phi = 15.0\%$ for small silica beads B30. The series is interesting because of the stresses which are considerably higher than the one of corresponding samples in other series and because it has a new feature in the small deformation limit. We have studied samples in a limited pH range, from pH 7.5 to 9.5. The low deformation part of the stress−strain curves is shown in Figure 5, with the complete curves in the inset. Let us start by discussing the small deformation regime ($\lambda < 1.3$): The break in slope which was already present in the $\sigma(\lambda)$ curve of the most acid sample at $\Phi = 5\%$ is seen to become more important and to be replaced by a well-defined maximum in stress for the lower pH values (pH $\approx$ 8). Its position varies somewhat with pH ($\lambda_{max} = 1.1-1.25$). Note that even for more "basic" films, there is still a prominent break in slope. This leads to Young's moduli scattered in the range from 20 to 35 MPa, i.e., up to about 20 times higher than the one of the pure nanolatex film. For the sample at pH 8.3, E is even as high as 40 MPa. In the high deformation regime ($\lambda > 1.3$), the stress of all samples of the series looks essentially like the one at $\Phi = 5.0\%$ shifted to higher values. All films break at elongations scattered between $\lambda_{rupt} \approx 3.3$ and 5, a bit earlier than the samples at $\Phi =$

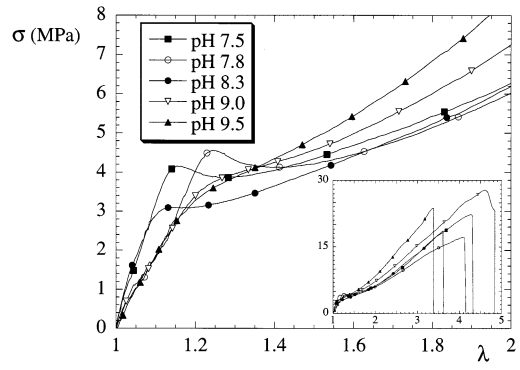

Figure 5. Stress σ in MPa as a function of relative elongation λ for nanocomposite films of silica B30 at $\Phi = 15.0\%$ for different pH values, for $1 < \lambda < 2$. Inset: the complete data set up to rupture. The sample at pH 9 did not break instantaneously.

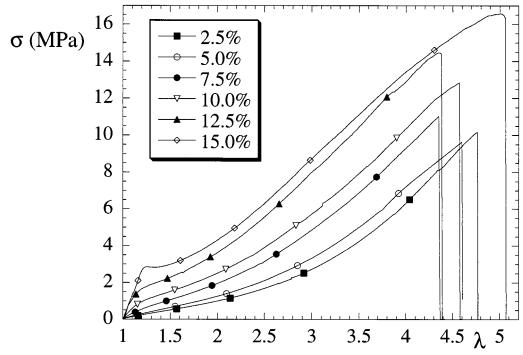

Figure 6. Stress σ in MPa as a function of relative elongation λ for nanocomposite films of silica B30, pH = 9.0, for different volume fractions Φ.

5.0% in the same pH range. This gives values of the energy per unit volume of film supplied up to rupture scattered around $e \approx 12$ J/cm^3.

To summarize, at $\Phi = 5\%$ the pH has an important effect on the rheological properties of the samples. The strongest reinforcement, expressed in terms of the ratio of Young's moduli of the composite and the pure matrix E/E_{latex}, is observed at low pH. The sample of highest E is also the one where a characteristic break in slope at small λ is observed. The results for higher volume fractions, $\Phi = 15\%$, show an even stronger reinforcement effect, with the particular feature of a maximum in stress at low deformations.

III.3. Effect of Silica Volume Fraction Φ and of the Silica/Latex Size Ratio. The comparison of the $\Phi = 5.0\%$ and $\Phi = 15.0\%$ series discussed above gives some idea about the influence of the silica volume fraction, and we now turn to a more detailed study. The stress−strain isotherms of a series of samples at fixed pH 9.0, and increasing volume fractions of silica (Φ = 2.5−15.0%) are shown in Figure 6. At small deformations, a break in slope is seen to emerge with increasing silica volume fraction, around $\lambda = 1.2$. At 15.0%, this break in slope becomes even a maximum. It is correlated with a high increase in Young's modulus: $E = 1.3$ MPa at $\Phi = 2.5\%$, 2.0 MPa at $\Phi = 5.0\%$, 6.7 MPa at 10.0%, up to 16 MPa at 15.0%. It is interesting to note that the reinforcement factor E/E_{latex} increases strongly, nonlinearly, with the silica volume fraction Φ. At larger deformation, the curves are roughly parallel, and rupture occurs between $\lambda_{rupt} = 4.3$ and 5.1. This shows again that one can stretch the nanocomposite films further than the pure nanolatex film at the same pH.

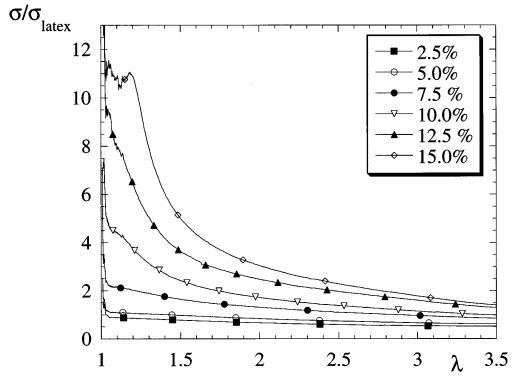

Figure 7. Reduced stress σ/σ_{latex} as a function of relative elongation λ for nanocomposite films of silica B30, pH = 9.0, for different volume fractions Φ.

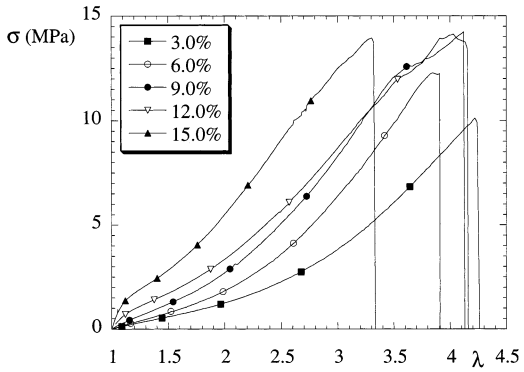

Figure 8. Stress σ in MPa as a function of relative elongation λ for nanocomposite films of silica B40, pH = 9.0, for different volume fractions Φ.

The energy needed to break the films in uniaxial extension increases also considerably with volume fraction: from 3.9 J/cm^3 ($\Phi = 5.0\%$) to 6.4 J/cm^3 ($\Phi = 10.0\%$) and 11.2 J/cm^3 at $\Phi = 15.0\%$. It is again interesting to plot the reduced stress σ/σ_{latex} as a function of elongation for different volume fractions (see Figure 7). At low volume fractions there is hardly any effect, and the curves are flat. At highest Φ, the peak emerges at low deformations, around $\lambda = 1.20$. At higher elongation, the reinforcement factor decreases quickly, down to a reinforcement of less than 2 at rupture. Note that the data are necessarily scattered at very low deformations, the relative stress there being a ratio of two small numbers affected by statistical errors.

We now explore the influence of the size of the silica beads by replacing the smaller silica B30 ($R_0 = 76.9$ Å) by silica B40 ($R_0 = 92.6$ Å, cf. section II) in the previous series in volume fraction Φ, at pH 9.0. The rheological response in terms of $\sigma(\lambda)$ is shown in Figure 8. The general behavior is the same for B40 and B30 (cf. Figure 6): The stress is of the same order of magnitude (σ_{rupt} = 10−15 MPa), and it increases considerably with the volume fraction. The samples break somewhat earlier for the bigger silica spheres (B40): λ_{rupt} lies between 3.3 and 4.3. The break in slope at low deformation, however, is less pronounced and seems to exist only at the highest volume fraction (Φ = 15.0%), if at all. Young's modulus varies strongly with Φ: from $E = 1.5$ MPa at $\Phi = 3.0\%$, it becomes 1.8 MPa at $\Phi = 6.0\%$, 3.3 MPa at 9.0%, 6.9 MPa at 12.0%, and 15.5 MPa at 15.0%. Simultaneously, the energy necessary to break the film about doubles from 3.6 J/cm^3 at $\Phi = 3.0\%$ to 6.8 J/cm^3 at $\Phi = 15.0\%$. In Figure 9, we plot the reinforcement

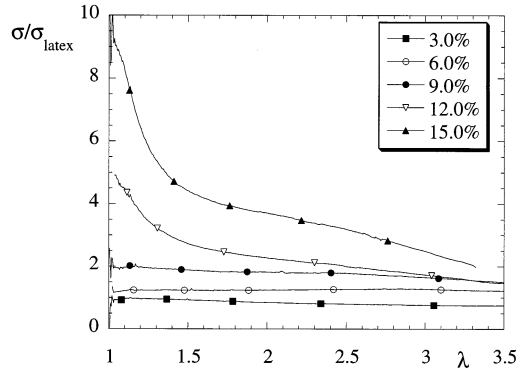

Figure 9. Reduced stress σ/σ_{latex} as a function of relative elongation λ for nanocomposite films of silica B40, pH = 9.0, for different volume fractions Φ.

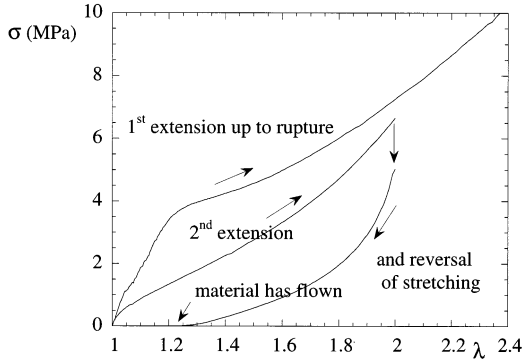

Figure 10. Stress σ in MPa as a function of relative elongation λ for a nanocomposite film of silica B30, pH = 9.0, Φ = 15.0%. First extension up to rupture ($\lambda_{rupt} = 4.6$), followed by a free relaxation. Then second extension up to $\lambda = 2.0$ and retraction back to $\lambda = 1.0$. See text for details.

factor σ/σ_{latex} as a function of elongation. At low volume fraction, Φ ≤ 9.0%, the reinforcement factor is essentially constant with λ. Its value is about 1 for Φ = 3.0%, 1.2 for Φ = 6.0%, and 2 for Φ = 9.0%. At higher volume fractions, a strong decrease of the reinforcement factor at low deformation is found. The sample at Φ = 12.0% starts with a factor of reinforcement of 4.8 and falls off to a plateau at 1.5. For the most concentrated sample, at Φ = 15.0%, it starts from a height close to 10 and reaches a value of 2 at large deformation. To summarize, the following differences with the analogous data series for small silica B30 (cf. Figure 7) are found: Samples with bigger silica beads break earlier, no peak is observed in the low deformation part, less energy is needed to extend the sample up to rupture, and Young's modulus or the reinforcement factor at low deformation is weaker.

III.4. A Double Elongation Experiment. In the series of rheological data which we have presented above, probably the most intriguing feature is the break in slope of σ at small deformations, around $\lambda = 1.2$. In the early stages of deformation, Young's modulus is very high, and suddenly, after some 15 or 20% of extension, the stress increases less steeply. The resulting break in slope exists either at the highest filler volume fraction, or if the pH of the colloidal precursor solution is low, or both. Alternatively, in the reinforcement factor presentation, the reduced stress starts from a high value and decreases quickly with elongation, before reaching a plateau. This plateau value shows still an important reinforcement effect that depends on the silica volume fraction and the pH, but it is clearly considerably weaker than the maximum height. It is tempting to associate this decrease with elongation at low λ with the destruction or reorganization of some hard filler structure during the very early stages of deformation. We will further exploit this idea in the Discussion. To test it, we have performed a *double elongation experiment* with one specific sample (Φ = 15.0%, pH 9.0, B30) which presents the break in slope. The result is shown in Figure 10. First, the film has been extended up to rupture (first extension). It was then given time to relax for 1 day at 60 °C (first retraction, not shown because immediately following the rupture), taken out, and a new clamp was fixed at the broken end of the sample. This "new" sample was then stretched a second time, up to $\lambda = 2.0$ with respect to its new length (second extension). Immediately afterward, the direction of motion was reversed, and the a third stress curve from $\lambda = 2.0$ to $\lambda = 1.0$ was measured (second retraction). From these data, two points become obvious: First of all, the prominent break in slope observed during the first extension has completely disappeared in the second one, although the stress around $\lambda = 2.0$ is comparable in both cases. A second, minor point is that the stress falls down to zero during the third (retraction) experiment before reaching $\lambda = 1$, which indicates of course that our samples undergo some viscous flow during the experiment and that the equilibrium length after stretching and relaxation is greater than the initial equilibrium length.

To verify that the observed behavior is not due to the latex, we have performed a similar double elongation experiment with a pure latex film. We find some minor differences between the stress during the first and second elongation, of the order of 5% in stress, which are by no means comparable to the differences observed with the nanocomposite sample.

IV. Discussion

IV.1. General Remarks on the Filler Structure. We have seen before[23] that the structure of the model nanocomposite films varies with the physicochemical conditions in solution before film formation. We have quantified the different structures in terms of the average aggregation number N_{agg}, which we have deduced from the peak position of the scattered intensity (cf. section IV.3 and ref 23). The general trend is that **(**a**)** N_{agg} is mainly determined by the pH, lower pH giving bigger aggregates, and **(**b**)** increasing the silica volume fraction Φ affects N_{agg} only partially, in the sense that the order of magnitude of N_{agg} is unchanged and the number of aggregates increased, and **(**c**)** bigger silica spheres aggregate less than the smaller ones. We recall that our explanation is that the equilibrium between attractive and short-ranged van der Waals forces and long-ranged electrostatic repulsion in solution depends on Φ and pH. At low pH, the OH surface groups of the latex (methacrylic acid) and the silica (silanol) are less ionized. This weakens the colloidal stability, and the resulting aggregation (or precipitation) of the silica is frozen in by the coalescence and film formation of the latex particles. This leads to an organization of the silica in the final film, after evaporation, which depends on the conditions in solution. We now confront the resulting structure to the rheological data presented in section III.

Table 1. Comparison of the Rheological Properties of the Pure Matrix and of Nanocomposites of the Series in pH, Silica B30, Φ = 5.0%[a]

	acid	neutral	basic
structure: N_{agg}	>5500	≈100	≈4−8
pure matrix			
E_{latex} (MPa)	0.45	1.05	1.45
σ_{rupt} (MPa)	<2	5.7	9.1
λ_{rupt}	>7	5.2	3.7
nanocomposite samples, Φ = 5.0%, B30			
E (MPa)	10.6	4.8	2.1
σ_{rupt} (MPa)	<3	7.5	10.1
λ_{rupt}	>8	5.5	4.5
E/E_{latex}	23.6	4.6	1.4

[a] The average number of aggregation is deduced from the SANS data. At pH 3.9, the estimated number of aggregation is greater than 5500.

IV.2. Effect of pH at Low Silica Volume Fraction. Of all the samples studied, the series in pH with silica B30 (Φ = 5.0%) presents the most striking changes in structure. At high pH, the aggregation number ranges from 4 to 8, whereas an estimation of several thousand is found at low pH. In Table 1 we compare the rheological properties of the pure matrix and of nanocomposites of this series. The evolution of E is opposite to the one of pure nanolatex films, indicating that the presence of filler leads to a qualitatively new rheological behavior. There is a clear correlation between the structure of the filler and the factor of reinforcement at small deformations. Both are determined by the pH, and the reduced modulus E/E_{latex} increases as N_{agg} increases, at constant volume fraction. The stress σ_{rupt} and the relative elongation at rupture λ_{rupt}, however, follow more or less the properties of the pure matrix. This evolution of the rheological properties from strong reinforcement at low λ to normal matrix properties at high λ can be seen in Figure 4, where the reinforcement factor is seen to decrease considerably for low pH values. It thus looks like the structure of the filler (quantified by N_{agg}) is reorganized with increasing strain, and the response at high deformation and the maximum elongation are mainly those of the matrix.

The importance of the interaction at the polymer−silica interface can be estimated by comparing the reinforcement factor at small and high deformation. Indeed, one might expect this interaction to be influenced by pH due to the different degree of electrostatic charging in solution and the resulting presence of ions in the film; e.g., the silica beads might be better connected to the matrix at high pH by ionic bridging. These effects are thought to persist at high deformation, as unbinding of polymer from these very small beads is known to be virtually impossible.[30] The ratio of (σ/σ_{latex}) at $\lambda = 1$ and at $\lambda = \lambda_{rupt}$, for the "acid" film in Figure 4 of the order of 10, indicates clearly that any surface interaction effect of pH is of second order with respect to structural differences between samples at different pH.

IV.3. Effect of pH at High Silica Volume Fraction. In Table 2 the average number of aggregation N_{agg} deduced from small-angle neutron scattering experiments using the same method of analysis as before[23] is given for the series in pH (silica B30, Φ = 15%). N_{agg} is seen to decrease monotonically with increasing pH, from about 42 down to below 10 at high pH. The rheological response of the samples presents the peak in stress at small deformations at lower pH and a pronounced break in slope at higher pH (cf. Figure 5). The rheological data

Table 2. Average Number of Aggregation N_{agg} Deduced from Small-Angle Neutron Scattering Experiments for Φ = 15.0%, Small Silica Beads B30, for Different Values of pH[a]

series in pH, B30, Φ = 15.0%	N_{agg}	λ_{max}	η (%)
pH = 7.5	42 ± 10	1.16	36
pH = 7.8	25 ± 5	1.24	40
pH = 8.3	12 ± 3	1.13	34
pH = 9.0	10 ± 3	1.22	39
pH = 9.5	<10	1.21	38

[a] See ref 23 for details. λ_{max} is the position of the maximum of the stress−strain curve, and η is the compacity of aggregates deduced from eq 9. Error bars are due to the limited resolution in the SANS experiments.

for this series are far from being uniform. There is no clear dependence on pH neither of Young's modulus (scattered between 20 and 40 MPa) nor of the stress at rupture (between 17 and 28 MPa) or elongation at rupture (between 3.3 and 5). In addition to this, the position of the maxima and breaks in slope does not vary monotonically with pH. They are located between λ = 1.10 and 1.25. It is therefore difficult to correlate these rheological properties with the structure of the samples, which varies in a more systematic manner with the pH (cf. Table 2). The only thing one might conclude at these high volume fractions is that there is considerable reinforcement, but the rheological properties do not seem to depend strongly on pH, besides the peaks in stress that exist only at low pH.

We have developed a simple geometric model relating the maximum of stress to the compacity of aggregates. The entire aggregate is thought to be contained in a sphere of radius R_{agg}. The ratio of the volume of silica in the aggregate and the volume of the sphere defines the compacity η:

$$\eta = \frac{N_{agg} V_{si}}{\frac{4\pi}{3} R_{agg}^{3}} \tag{5}$$

V_{si} is the average volume of a silica bead. The model is based on the fact that aggregates are well dispersed in space, which is known from the scattering experiments. Indeed, the repulsion between them leads to a strong scattering peak. The picture developed here applies only in the early stages of deformation, up to collision between aggregates. It is a mean-field model, by taking the equilibrium interaggregate distance as a constant; i.e., all fluctuations in size and position are ignored.

We interpret the low deformation maximum in the stress $\sigma(\lambda)$ discussed in section III as the result of collisions between aggregates. When two aggregates collide, the polymer between them is subjected to high compression, thereby increasing the macroscopic stress. As soon as the local stress between aggregates exceeds some critical value, aggregates need to be reorganized in the matrix (e.g., turn around each other, break up, etc.). This would result in a local relaxation of polymer, decrease the macroscopic stress, and thus explain the observed maximum.

Aggregates are supposed to be identical in compacity and aggregation number, with an average initial center-to-center distance D_0 deduced from the position q_0 (in Å^{-1}) of the scattering peak, $D_0 = \alpha 2\pi/q_0$; cf. ref 23 for details. α is a constant, a priori unknown, which quantifies the interaggregate structure. For a cubic

arrangement of aggregates, α would be 1. The aggregation number is determined from D_0 and the knowledge of V_{si} (determined independently):

$$N_{agg} = \frac{D_0^3 \Phi}{V_{si}} \tag{6}$$

It can be supposed that aggregates start by following the polymer matrix and thus the macroscopic displacement affinely.[1] Under uniaxial strain, an elongation λ along z of the incompressible sample leads then to the following equations of motion of the center of an aggregate initially located at (x_0, y_0, z_0) in a Cartesian coordinate system:

$$x = \frac{x_0}{\sqrt{\lambda}}$$

$$y = \frac{y_0}{\sqrt{\lambda}}$$

$$z = \lambda z_0 \tag{7}$$

Collisions will occur for the first time between aggregates in the xy plane, where the distance between two aggregates evolves according to (see Appendix for details)

$$D = D_0/\lambda^{1/2} \tag{8}$$

On average, aggregates touch when the center-to-center distance equals two aggregate radii, $D = 2R_{agg}$. We arbitrarily identify this moment with the maximum in stress, which occurs at $\lambda = \lambda_{max}$, and combining eqs 5, 6, and 8 gives the following result (cf. Appendix):

$$\eta = \frac{6\Phi}{\pi} \lambda_{max}^{3/2} \tag{9}$$

Note that it is independent of α, because η is a ratio between the total volume and the volume of silica of the aggregates, both estimated from the scattering wave vector q_0. The limitations of this simple model are obviously that aggregates are probably neither all identical nor equally spaced in the matrix. The model does not allow to estimate the observed stress either, as no constitutive rheological equation is included. It allows us to link the strain value at the maximum to the compacity of the aggregates. The results are given in the fourth column of Table 2. They vary from 34% to 40%. It can easily be seen that these are reasonable values, e.g., in the case of pH 9 by constructing a simple aggregate with $N_{agg} = 10$: nine spheres of radius R can be aggregated in one layer around a central one, the maximum radius of the aggregate being simply $3R$. The compacity is obtained by dividing 10 bead volumes $10 \times 4\pi R^3/3$ by the volume of the aggregate, and we obtain a compacity of $\eta = 37\%$. In a similar way, a compacity of 34% is found for the sample at pH 7.5 ($N_{agg} = 42$), which is close to the value deduced from the model (36%). In conclusion, this would indicate that aggregates are rather compact (not tenuous), although not close-packed.

IV.4. Comparison between Small (B30) and Bigger (B40) Silica Beads. We now turn to the series in Φ, at pH 9.0, which exists for both the smaller (B30) and the bigger (B40) silica beads. We have seen in our previous article that samples of the series in Φ at pH 9.0, with silica beads B30, have an average number of aggregation of the order of 10. In the case of the bigger silica beads (B40), the neutron scattering results indicate rather little aggregation at this pH: N_{agg} is between 1 and 2. In the SANS spectra a small-q upturn indicates the presence of bigger aggregates, which are so rare that their contribution to the total stress is probably negligible. The important result of the structural study is that the numbers of aggregation do not change significantly with Φ in the two systems and that there is at least 5 times higher aggregation in the case of the smaller silica beads.

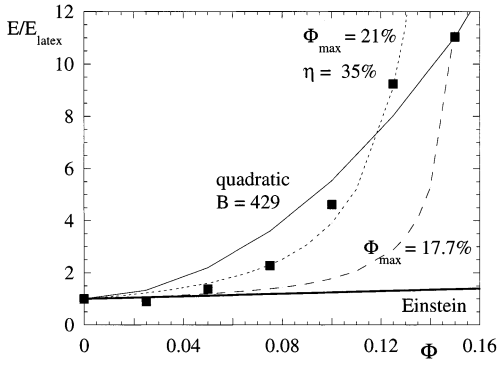

Figure 11. Reinforcement factor E/E_{latex} for the series in silica volume fraction Φ at pH 9.0 for the small silica beads B30 (squares). Model calculations are the linear Einstein equation (eq 3a, thick solid line), the quadratic one (eq 3b, solid line), the packing model (eq 4b, broken line), and the packing model with compacity (eqs 4b and 10, dotted line).

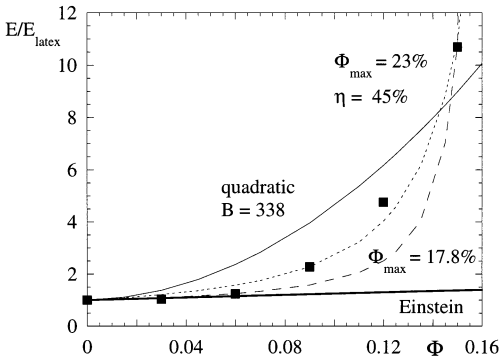

Figure 12. Reinforcement factor E/E_{latex} for the series in silica volume fraction Φ at pH 9.0, for the bigger silica beads B40 (squares). Model calculations are the linear Einstein equation (eq 3a, thick solid line), and the quadratic one (eq 3b, solid line), the packing model (eq 4b, broken line), and the packing model with compacity (eqs 4b and 10, dotted line).

We first focus on the evolution of the low deformation response with volume fraction, which we confront with the theoretical models described in eqs 3 and 4. In Figures 11 and 12, we have plotted the ratio E/E_{latex} as a function of volume fraction for the B30 and B40 samples, respectively. In the rheological response of these systems, the main difference seems to be the rather weak break in slope in $\sigma(\lambda)$ at small deformations for the B40 system, whereas it is clearly visible for $\Phi = 12.0\%$ in the B30 system and becomes even a maximum at $\Phi = 15.0\%$. The fact that the series with the small silica develops quickly the break in slope can be seen by the jump in E/E_{latex} between 9% and 12%, after which E/E_{latex} seems to level off (Figure 11). The series with the bigger silica beads reaches about the same final

value of E/E_{latex} at $\Phi = 15\%$, but apparently more progressively (Figure 12).

Our first verification was to test the Einstein equation, eq 3a, and its extension to higher volume fractions, eq 3b. Both functions are shown in Figures 11 and 12. Not surprisingly, Einstein's equation (thick lines) is below the data set as soon as the volume fraction exceeds some 5%. If the extension to second order, eq 3b, is used, the prefactor B has to be chosen absurdly high in order to meet at least the order of magnitude of E/E_{latex} at $\Phi = 15\%$. This is plotted in thin continuous lines in the figures, with $B = 429$ for B30 and $B = 338$ for B40. It is obvious that the data are not well described by eqs 3a and 3b. The same is true for eq 4a, which superimposes with the original Einstein equation within a few percent on the whole range shown here and thus severely underestimates the experimental data for $\Phi > 5\%$. The percolation approach, eq 4b, does a bit better then the other models. Fitting it to the data, however, yields rather low packing volume fractions Φ_{max} between 17% and 18%. The quality of the fits is not very good; the data are underestimated up to a violent divergence when approaching 15% (broken lines in Figures 11 and 12).

Given the poor performance of the standard models, an obvious way to improve them is to take the compacity of the aggregates into account. It is well-known that aggregates contain occluded and/or bound rubber, which is blocked inside (or on the surface of) the aggregates and behaves as hard filler.[31−33] Thus, bound rubber increases the efficient volume of the aggregates, and the total volume fraction of filler plus bound rubber in aggregates Φ_{agg} can be expressed through the compacity η as defined in eq 5:

$$\Phi_{agg} = \frac{\Phi}{\eta} \tag{10}$$

We now identify the silica volume fraction Φ in eqs 3 and 4 with the aggregate volume fraction Φ_{agg} and leave η as a free parameter for a fit. The linear Einstein equation, eq 3a, of course, stays linear and cannot account for the observed nonlinearity of the data. The shape of the curve predicted by the extension of Einstein's equation to second order, eq 3b, with B fixed to 14.1, is too weakly curved compared to the data (not shown in the figures). It overestimates the low-Φ data by a factor of 2 and the corresponding compacities, $\eta = 20\%$ and 23% for B30 and B40, respectively, are rather low. The exponential function, eq 4a, has the same flaws as eq 3b: It overestimates the low-Φ data by almost a factor of 2 and predicts η values between 15% and 17% (not shown).

The prediction of eq 4b, finally, is closest to the data. Let us go back to the case of E/E_{latex} of B30, shown in Figure 11. The relatively weak increase between 12% and 15% is impossible to reproduce with any of the equations proposed here. We have therefore fitted two data sets, one with and one without the data point at $\Phi = 15\%$. It is found that the data set without the last point can be described with $\Phi_{max} = 21\%$ and $\eta = 35\%$, which corresponds to a packing fraction of aggregates $\Phi_{agg,max}$ of $\Phi_{max}/\eta = 60\%$, a reasonable value. The resulting curve is plotted in Figure 11 (dotted line), and the agreement is acceptable. Including the last point leads to fits of the (low) quality of the quadratic expression, eq 3b, with unreasonable parameter values ($\Phi_{max} > 100\%$, not shown in the figure).

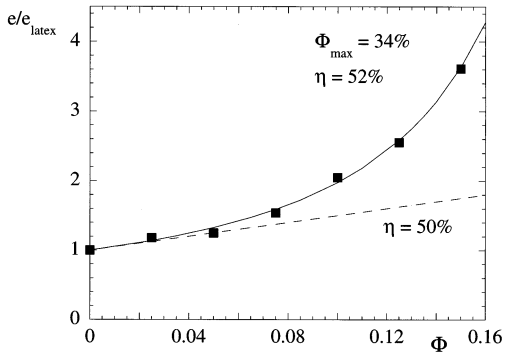

Figure 13. Reduced energy up to rupture e/e_{latex} as a function of silica volume fraction Φ for small silica beads B30 at pH 9.0. The broken line is the prediction of the Einstein equation (eq 3a) and the solid line that of the packing model (eq 4b), both combined with eq 10.

The complete data set of the B40 series as plotted in Figure 12 have also been fitted with eq 4b, with the substitution of Φ by $\Phi_{agg} = \Phi/\eta$ (eq 10). The result (dotted line) has been obtained for $\Phi_{max} = 23\%$ and $\eta = 45\%$. Considering that the aggregates are smaller (N_{agg} between 1 and 2) and that smaller aggregates have usually a higher compacity (an aggregate made of a single bead has a compacity of $\eta = 100\%$), the value of 45% for η seems acceptable. The same is true for the aggregate packing volume fraction, which turns out to be $\Phi_{agg,max} = \Phi_{max}/\eta = 51\%$.

We have just seen that the low deformation response, a strong increase of E with Φ, can be described by the diverging "packing" (or percolation) term. As we have also seen before (cf. Figures 7 and 9), even initially very high reinforcement factors decrease considerably with deformation. It is therefore interesting to study the evolution with volume fraction of a quantity which rationalizes the reinforcement effect over the complete deformation range. We have tried to do this with the energy per unit volume of sample needed to break the film, as defined in eq 2. Although there are some problems with the energy, mainly due to the fact that rupture occurs in an uncontrolled manner, we present in Figure 13 the reduced energy e/e_{latex} as a function of silica volume fraction Φ for the small silica beads B30. In the absence of any complete theory for the stress−strain function of nanocomposite samples, we compare it to the predictions of eqs 3a and 4b for the relative modulus E/E_{latex}.[28] The substitution of Φ by Φ_{agg}, eq 10, is again included. At low deformations, eq 3a does a good job provided that the compacity of the aggregates is set to $\eta = 50\%$ (broken line in Figure 13). A fit with eq 4b yields a good description of the data, with $\eta = 52\%$ and $\Phi_{max} = 34\%$; thus $\Phi_{agg,max} = 65\%$, a reasonable value (solid line in Figure 13).

We have analyzed the energy up to rupture for the bigger silica beads B40 in an analogous manner. The results, plotted in Figure 14, are rather different from the B30 case. Namely, the rather low value at $\Phi = 15\%$ makes satisfactory fitting with the functions at hand, eqs 3 and 4, impossible. A tentative fit in the low-Φ region with the Einstein equation (including eq 10) yields a compacity of $\eta = 45\%$, close to the previously determined value (broken line in Figure 14). Setting η to 45% and the packing volume fraction to 34% as in the case of B30 gives the solid line, which of course is not satisfying because it does not describe the high-Φ part well.

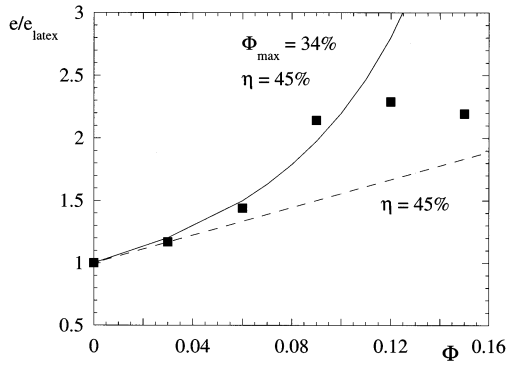

Figure 14. Reduced energy up to rupture e/e_{latex} as a function of silica volume fraction Φ for small silica beads B40 at pH 9.0. The broken line is the prediction of the Einstein equation (eq 3a) and the solid line that of the packing model (eq 4b), both combined with eq 10.

For the sake of completeness, we wish to mention two alternative calculations relevant for the rheology of aggregates suspended in a matrix. The first is the self-consistent viscosity calculation by Potanin.[34] Its low-shear, low-volume fraction limit gives a result which can essentially be looked at as a combination of the second-order Einstein equation, eq 3b, with a percolation term like the one in eq 4b and the volume fraction of aggregates determined by eq 10. The second is the model developed by Witten et al.[35] In their analysis of the reinforcement of elastomers by fractal aggregates, they start with an expression for the modulus as a function of volume fraction. This equation predicts a rather high power in Φ, between $\nu = 3.3$ and 4.4, depending on the fractal dimension and connectivity exponent of the aggregates. We have compared the data presented in Figures 11 and 12 to this prediction ($E/E_{latex} = 1 + a\Phi^{\nu}$) and obtain good fits for exponents of $\nu = 3.65$ (for B30, neglecting the point at $\Phi = 15\%$) and of $\nu = 4.14$ (B40). This is in line with our results, as it corresponds to a higher fractal dimension in the case of B40, i.e., a higher compacity. One should not overestimate this finding, though, because the calculation is based on the mathematical concept of fractals, which probably does not apply to our case of rather small aggregates. On the other hand, the underlying physics in both cases is the approach of percolation of aggregates, which is responsible for the steep increase of the modulus with silica volume fraction.

IV.5. Criticism of the Data and a Tentative Scenario. Before turning to a tentative picture coherent with all observations, we discuss the quality of the data, which do not always behave as it would be convenient for a straightforward interpretation. There are two types of problems. The first one is the obvious statistical nature of the rupture process, which leads to a large scattering of the stress and strain at rupture, and the total energy supplied up to rupture. The second one is the presence of apparent incoherences in the data, like inversions with respect of the nominal order of a series. The system under study being complex enough, it can a priori not be excluded that there is a physical reason for these deviations. It has to be recognized, however, that identical physicochemical manipulations (like deionization) of the stock solutions of industrial origin may not always lead to exactly the same result, namely concerning the concentration of ionic species.[36] The same might be true for the exact gelation time of the sample before film formation. Nevertheless, once the film is formed with a given number of aggregation, it has a clear rheology−structure relationship. We are therefore convinced that the main conclusions of the article are not affected despite these shortcomings. Let us now summarize the key points of the data presented here and in the structural study:

(i) At low volume fractions, with decreasing pH, the average aggregation number and the reduced modulus E/E_{latex} increase considerably.

(ii) At higher volume fractions, the aggregation number still increases with decreasing pH, but the stress−strain curves are less systematic. At lower pH, a maximum in stress at low deformations is observed. This maximum can be linked to a compacity of aggregates of the order of 35% by a geometric model.

(iii) Small beads at basic pH aggregate ($N_{agg} \approx 10$) more than the bigger ones ($N_{agg} \approx 1-2$). The reinforcement factor of films made with small beads (B30, $\Phi = 15\%$) is very high at low deformations, presents a maximum, and then decreases quickly. The one of films made with the bigger beads is weaker, has no maximum, and decreases less rapidly.

(iv) The break in slope disappears after a first elongation up to rupture (double elongation experiment).

(v) The evolution of the reduced modulus E/E_{latex} with volume fraction can be understood with a packing model ($\Phi_{max} = 21\%$) and an aggregate compacity of 35% in the case of B30. For B40, the values are $\Phi_{max} = 23\%$ and $\eta = 45\%$. The evolution of the reduced energy e/e_{latex}, which takes the complete stress−strain curve into account, indicates higher compacity after deformation in the case of B30 and unchanged compacity for B40.

We propose the following tentative scenario. Two types of dissipative processes have to be considered. The first is breaking up of aggregates, and the second is reorganization of relative aggregate positions, accompanied by stress relaxation. Bigger aggregates break up more easily than smaller ones, and breaking up of aggregates is considered irreversible. The bigger the aggregates, the more energy is spent in the first stages of deformation to break them up. Young's modulus increases accordingly with the aggregation number. If the aggregates are close enough (high volume fraction), this is accompanied by collisions and spatial reorganization of the filler structure. After deformation up to rupture, aggregates will be smaller and more compact, and a second elongation will not bring them in contact any more. In the case of small aggregates (B40, basic pH), the compacity is higher from the beginning. Upon deformation aggregates can only reorganize spatially, without any breaking up of aggregates because they are small, which explains why the reduced stress decreases less steeply with B40 than with B30. The compacity of the B40 aggregates is thus unchanged.

V. Conclusion

We have studied the rheological properties of a special nanocomposite material, obtained by film formation of mixtures of colloidal silica and nanolatex solutions. The stress−strain isotherms show considerable sensitivity to the physicochemical parameters of the solutions before film formation, namely pH, silica volume fraction, and silica bead size. At low silica volume fraction, for instance, the small deformation behavior (Young's modulus) depends in a crucial way on the pH, such that samples of identical silica volume fraction can differ by as much as a factor of 5 in the modulus. By leading our

investigation in parallel with a small-angle neutron scattering study of the structure at rest, it is also found that the rheological properties are correlated with the degree of aggregation.

We have analyzed our data in three different ways. The first and most important one is to normalize the stress by the stress of the pure matrix formed at the same pH. This allows us to conclude on a strain-dependent reinforcement factor, independent of the matrix properties. It is found that the reduced stress is high at low pH and small deformation and that it decreases with increasing strain. Second, we have analyzed the dependence of Young's modulus on silica volume fraction at a fixed pH. This dependence is stronger than the one predicted by the first-order Einstein equation, nonlinear, and compatible with a packing model. Third, we have tried to analyze a global parameter, the energy supplied up to rupture, as a function of silica volume fraction. The data demonstrate again the high reinforcement obtained with the smaller silica beads. Moreover, it gives some indication on compactification of big aggregates during sample deformation.

Many aspects are still to be explored in the nanocomposite system presented here. Changes in structure during deformation, e.g., could in principle be detected by small-angle neutron scattering experiments. One remarkable result, however, is out of question: the rheological properties of the nanocomposites can be tuned over a large range, without chemically modifying the silica surface.

Acknowledgment. We are indebted to Jean-Christophe Castaing (Rhodia) for offering us the nanolatex and to Akzo Nobel for the silica. The work presented here has benefited from interesting discussions with François Boué and Annie Brûlet. The latter has also written the software for the stretching apparatus. During a stay at our laboratory, Laurent de la Réberdière has measured some of the stress−strain isotherms of pure nanolatex.

Appendix

The initial distance D_0 between aggregates i located at (x_i,y_i) in the xy plane reads

$$D_0 = [(x_1 - x_2)^2 + (y_1 - y_2)^2]^{1/2} \quad \text{(A.1)}$$

After affine deformation (eq 7) the distance becomes

$$D = \left[\left(\frac{x_1}{\sqrt{\lambda}} - \frac{x_2}{\sqrt{\lambda}}\right)^2 + \left(\frac{y_1}{\sqrt{\lambda}} - \frac{y_2}{\sqrt{\lambda}}\right)^2\right]^{1/2} = \frac{D_0}{\sqrt{\lambda}} \quad \text{(A.2)}$$

Aggregates touch when their center-to-center distance D equals two aggregate radii:

$$D = 2R_{agg} = \frac{D_0}{\sqrt{\lambda_{max}}} \quad \text{(A.3)}$$

where we have identified this moment with λ_{max} in the second equality of (A.3). Rewriting eq A.3 yields

$$\left(\frac{D_0}{R_{agg}}\right)^3 = 8\lambda_{max}^{3/2} \quad \text{(A.4)}$$

Substituting N_{agg} from eq 6 in eq 5, we get

$$\eta = \frac{3\Phi}{4\pi}\left(\frac{D_0}{R_{agg}}\right)^3 \quad \text{(A.5)}$$

Substituting the expression for $(D_0/R_{agg})^3$ from eq A.4 in eq A.5 finally gives eq 9.

References and Notes

(1) *Science and Technology of Rubber*; Mark, J. E., Erman, B., Eirich, F. R., Eds.; Academic Press: San Diego, 1994.
(2) *Mechanical Properties of Polymers and Composites*; Nielsen, L. E., Landel, R. F., Eds.; Marcel Dekker: New York, 1994.
(3) Edwards, D. C. *J. Mater. Sci.* **1990**, *25*, 4175.
(4) Boonstra, B. B. *Polymer* **1979**, *20*, 691.
(5) Medalia, A. I. *J. Colloid Interface Sci.* **1970**, *32*, 115.
(6) Voet, A. *J. Polym. Sci., Macromol. Rev.* **1980**, *15*, 327.
(7) McCarthy, D. W.; Mark, J. E.; Schaefer, D. W. *J. Polym. Sci., Part B* **1998**, *36*, 1167.
(8) McCarthy, D. W.; Mark, J. E.; Clarson, S. J.; Schaefer, D. W. *J. Polym. Sci., Part B* **1998**, *36*, 1191.
(9) Matejka, L.; Dukh, O.; Kolarik, J. *Polymer* **1999**, *41*, 1449.
(10) Landry, C. J. T.; Coltrain, B. K.; Wesson, J. A.; Zumbulyadis, N.; Lippert, J. L. *Polymer* **1992**, *33*, 1496.
(11) Pu, Z.; Mark, J. E.; Jethmalani, J. M.; Ford, W. T. *Chem. Mater.* **1997**, *9*, 2442.
(12) Kraus, G. *J. Appl. Polym. Sci., Appl. Polym. Symp.* **1984**, *39*, 75.
(13) Payne, A. R. In *Reinforcement of Elastomers*; Kraus, G., Ed.; Interscience Publishers: New York, 1965.
(14) DeGroot, J. V.; Macosko, C. W. *J. Colloid Interface Sci.* **1999**, *217*, 86.
(15) Heinrich, G.; Vilgis, T. A. *Macromolecules* **1993**, *26*, 1109.
(16) Ehrburger-Dolle, F.; Hindermann-Bischoff, M.; Livet, F.; Bley, F.; Rochas, C.; Geissler, E. *Langmuir* **2001**, *17*, 329.
(17) Inoue, T.; Moritani, M.; Hashimoto, T.; Kawai, H. *Macromolecules* **1971**, *4*, 500.
(18) Rharbi, Y.; Joanicot, M.; Vacher, A.; Cabane, B.; Boué, F. *Europhys. Lett.* **1999**, *46*, 472.
(19) Rharbi, Y.; Boué, F.; Joanicot, M.; Cabane, B. *Macromolecules* **1996**, *29*, 4346.
(20) Winnik, M. A. *Curr. Opin. Colloid Interface Sci.* **1997**, *2*, 192.
(21) Joanicot, M.; Wong, K.; Cabane, B. *Macromolecules* **1996**, *29*, 4976.
(22) Dingenouts, N.; Ballauf, M. *Langmuir* **1999**, *15*, 3283.
(23) Oberdisse, J.; Demé, B. *Macromolecules* **2002**, *35*, 4397.
(24) Smallwood, H. M. *J. Appl. Phys.* **1944**, *15*, 758−766.
(25) Einstein, A. *Ann. Phys.* **1906**, *19*, 289.
(26) Guth, E.; Gold, O. *Phys. Rev.* **1938**, *53*, 322.
(27) Guth, E. *J. Appl. Phys.* **1944**, *16*, 20.
(28) Ahmed, S.; Jones, F. R. *J. Mater. Sci.* **1990**, *25*, 4933.
(29) Mooney, M. *J. Colloid Sci.* **1951**, *6*, 162.
(30) Gent, A. N. *J. Mater. Sci.* **1980**, *15*, 2884.
(31) Medalia, A. I. *Rubber Chem. Technol.* **1974**, *47*, 411.
(32) Polmanteer, K. E.; Lenz, C. W. *Rubber Chem. Technol.* **1975**, *48*, 795.
(33) Vidal, A.; Donnet, J. B. *Prog. Colloid Polym. Sci.* **1987**, *75*, 201.
(34) Potanin, A. A. *J. Colloid Interface Sci.* **1993**, *156*, 143.
(35) Witten, T. A.; Rubinstein, M.; Colby, R. H. *J. Phys. II* **1993**, *3*, 367.
(36) Note that this is not true for all parameters. The silica volume fraction, for example, is perfectly known (and confirmed by the high-q part of the SANS spectra).

MA020635D